

ARTICLE

Received 13 Jun 2016 | Accepted 13 Oct 2016 | Published 12 Dec 2016

DOI: 10.1038/ncomms13543

OPEN

Emergent Weyl excitations in systems of polar particles

Sergey V. Syzranov^{1,2,3,4}, Michael L. Wall^{2,3,†}, Bihui Zhu^{1,2,3}, Victor Gurarie^{1,2,3} & Ana Maria Rey^{1,2,3}

Weyl fermions are massless chiral particles first predicted in 1929 and once thought to describe neutrinos. Although never observed as elementary particles, quasiparticles with Weyl dispersion have recently been experimentally discovered in solid-state systems causing a furore in the research community. Systems with Weyl excitations can display a plethora of fascinating phenomena and offer great potential for improved quantum technologies. Here, we show that Weyl excitations generically exist in three-dimensional systems of dipolar particles with weakly broken time-reversal symmetry (by for example a magnetic field). They emerge as a result of dipolar-interaction-induced transfer of angular momentum between the $J=0$ and $J=1$ internal particle levels. We also discuss momentum-resolved Ramsey spectroscopy methods for observing Weyl quasiparticles in cold alkaline-earth-atom systems. Our results provide a pathway for a feasible experimental realization of Weyl quasiparticles and related phenomena in clean and controllable atomic systems.

¹Physics Department, University of Colorado, Boulder, Colorado 80309, USA. ²JILA, NIST, University of Colorado, Boulder, Colorado 80309, USA. ³Center for Theory of Quantum Matter, University of Colorado, Boulder, Colorado 80309, USA. ⁴Joint Quantum Institute, University of Maryland, College Park, Maryland 20742, USA. †Present address: The Johns Hopkins Applied Physics Laboratory, Laurel, MD 20723, USA. Correspondence and requests for materials should be addressed to S.V.S. (email: sergey.syzranov@googlemail.com) or to A.M.R. (email: arey@jilau1.colorado.edu).

Recent predictions^{1,2} and experimental observations^{3–5} of Weyl semimetals in solid-state systems have instigated intensive studies of their properties, such as non-local electrodynamics and chiral anomaly⁶, topologically protected Fermi arcs on the surfaces^{2,4,5}, non-Anderson disorder-driven transitions^{7–13} and unusual dependencies of transport properties on doping and temperature^{14–16}. In parallel, enormous research efforts are now directed at finding Weyl excitations in new systems. A promising platform for exploring Weyl physics is tunable and fully controllable ultracold atomic gases^{17–22}. However, henceforth proposed cold-atom realizations of Weyl quasiparticles have focussed mostly on non-interacting systems, and all have required implementations of externally imposed spin-orbit coupling through laser-assisted tunnelling schemes^{17–21}, other optical means^{23–25} or external rotating fields²².

In this paper we demonstrate that excitations with Weyl dispersion generically emerge in three-dimensional (3D) arrays of dipolar particles in the presence of a weak magnetic field, as a result of the dipole-interactions-induced transitions between their internal angular momentum $J=0$ and $J=1$ states. These excitations exhibit the same single-particle physics as Weyl fermions²⁶ but, similarly to other non-fermionic Weyl excitations³, their many-particle properties are expected to be different, opening alternative research directions, new functionalities and applications beyond those accessible with solid-state systems^{4,5}.

We also show that, experimentally such excitations can be observed, for instance, in trapped alkaline-earth atoms (AEAs) in a 3D optical lattice with lattice spacings smaller than the wavelength of the electronic $J=0$ to $J=1$ transition. The simple and unique internal structure of these atoms has already lead to record levels of precision and accuracy in atomic clocks²⁷. Taking advantage of the well developed spectroscopic tools to interrogate and manipulate AEAs, we propose to probe the Weyl quasiparticle dispersion and non-trivial chirality by means of momentum-resolved Ramsey spectroscopy. Our proposal opens a path for a feasible experimental realization of Weyl quasiparticles in clean and controllable atomic systems. Moreover, it lays the groundwork for the yet unexplored regime of topologically protected sensing, owing to the topological robustness of Weyl quasiparticles that could be used to push the stability and accuracy of optical lattice AEA-based clocks.

Results

Phenomenological argument. We assume that the system has long-lived excitations (quasiparticles) with (integer) angular momentum \mathbf{J} . Due to the translational invariance, the (quasi)-momentum \mathbf{k} is a good quantum number. In the long-wave limit the effective quasiparticle Hamiltonian is insensitive to the details of the potential of the periodic lattice that the particles may be placed in. To preserve rotation and inversion symmetries in the absence of magnetic field the Hamiltonian has to be an even function of $(\mathbf{k} \cdot \hat{\mathbf{J}})$ and a function of $|\mathbf{k}|$ and $\hat{\mathbf{J}}^2$. In the presence of a sufficiently weak uniform magnetic field, ω , that creates a perturbation $-\omega \cdot \hat{\mathbf{J}}$ independent of \mathbf{k} in the limit $\mathbf{k} \rightarrow 0$, the most generic form of the quasiparticle Hamiltonian is given by

$$\hat{h}(\mathbf{k}, \mathbf{J}) = F\left[|\mathbf{k}|, (\mathbf{k} \cdot \hat{\mathbf{J}})^2, \hat{\mathbf{J}}^2\right] - \omega \cdot \hat{\mathbf{J}}, \quad (1)$$

where F is an arbitrary function of three arguments.

The small quasimomentum \mathbf{k} can be measured from any high-symmetry point in the Brillouin zone characterized by an isotropic dispersion $\xi_{\mathbf{k}} = \xi(|\mathbf{k}|)$ of non-interacting particles in the limit $\mathbf{k} \rightarrow 0$.

For the particular case of $J=1$, the Hamiltonian (1) has nodes at momenta $\mathbf{K}|\omega$, such that $F(|\mathbf{K}|, |\mathbf{K}|^2, 2) \pm \omega = F(|\mathbf{K}|, 0, 2)$, corresponding to two intersecting branches with angular-momentum projections $J_z=0$ and $J_z=1$ or $J_z=-1$ on the direction of magnetic field. We note that such nodes always exist for weak magnetic fields and Hamiltonians that are regular as a function of \mathbf{k} .

The excitation Hamiltonian near a node is obtained by expanding the function F in small momentum $\mathbf{p} = \mathbf{k} - \mathbf{K}$. For a 3D system, it has Weyl dispersion of the form (see ‘Methods’ section):

$$\hat{h}_{\text{eff}}(\mathbf{p}) = \zeta(\mathbf{p}) + v_{\perp} \hat{\sigma}_x p_x + v_{\perp} \hat{\sigma}_y p_y + v_{\parallel} \hat{\sigma}_z p_z \quad (2)$$

with Pauli matrices $\hat{\sigma}_i$ acting in the space of the respective two angular-momentum projections.

Model. In what follows we confirm the above phenomenological argument by microscopic calculations for a 3D system of dipolar particles described by the Hamiltonian

$$\hat{H} = \sum_i \hat{H}_0(\mathbf{r}_i) + \frac{1}{2} \sum_{ij} \hat{H}_{\text{dip}}(\hat{\mathbf{d}}_i, \hat{\mathbf{d}}_j, \mathbf{r}_i - \mathbf{r}_j), \quad (3)$$

where $\hat{\mathbf{d}}_i$ is the dipole moment operator of the i -th particle, and

$$\hat{H}_0(\mathbf{r}_i) = -\frac{\nabla_i^2}{2m} + U(\mathbf{r}_i) + B_j \hat{\mathbf{J}}_i^2 - \hat{\mathbf{J}}_i \cdot \mathbf{B} \quad (4)$$

is the single-particle Hamiltonian that includes the particle kinetic energy $-\frac{\nabla_i^2}{2m}$ (hereinafter $\hbar = 1$), the periodic potential $U(\mathbf{r}_i)$ of the lattice that the system may be placed in, the energy $B_j \hat{\mathbf{J}}_i^2$ of internal levels with $\hat{\mathbf{J}}_i$ being the angular momentum of the i -th particle, and the interaction $-\hat{\mathbf{J}}_i \cdot \mathbf{B}$ with magnetic field (measured in units of the gyromagnetic ratio) that splits the $J=1$ levels.

The most generic form of the dipole-dipole interaction, which accounts for retardation effects, is given by ref. 28 (see also ‘Methods’ section)

$$\hat{H}_{\text{dip}}(\hat{\mathbf{d}}_i, \hat{\mathbf{d}}_j, \mathbf{r}) = a(r) (\hat{\mathbf{r}} \cdot \hat{\mathbf{d}}_i) (\hat{\mathbf{r}} \cdot \hat{\mathbf{d}}_j) + b(r) \hat{\mathbf{d}}_i \cdot \hat{\mathbf{d}}_j \quad (5)$$

where $\hat{\mathbf{r}} = \mathbf{r}/r$; $a(r) = \frac{3\gamma_0}{4d^2} [y_2(k_0 r) - ij_2(k_0 r)]$ and $b(r) = \frac{3\gamma_0}{4d^2} \sum_{n=0}^{\infty} (-1)^n [y_n(k_0 r) - ij_n(k_0 r)] / (k_0 r)$ for $r \neq 0$, with y_n and j_n being the n -th-order spherical Bessel functions of the second and first kind respectively and k_0 —the wavevector of the $J=0$ to $J=1$ transition. The terms proportional to y_n describe elastic interactions between dipoles a distance r apart, while the terms with j_n account for the inelastic collective photon emission (radiation). $\gamma_0 = \frac{k_0^3 d^2}{3\pi\epsilon_0}$ is the natural linewidth of the transition and d is its dipole moment. If the dipoles are much closer to one another than the wavelength of the dipole transition, $k_0 r \ll 1$, retardation effects can be ignored, and one recovers the more familiar form of the dipolar interactions, $a(r) \propto -3/r^3$, $b(r) \propto 1/r^3$, common for NMR solid-state systems²⁹, polar molecules³⁰ and Rydberg atoms^{31,32}.

We note that the above phenomenological derivation of the dispersion of Weyl-type quasiparticles carries over straightforwardly to other dimensions. For example, a 2D system of dipolar particles with an in-plane magnetic field hosts 2D Dirac excitations with the dispersion of monolayer graphene³³. We emphasize that such 2D excitations are distinct from the 2D ‘chiron’ excitations³⁴ that exist in a perpendicular magnetic field and resemble electrons in bilayer graphene.

Atoms in a deep lattice. While the above phenomenological argument demonstrates the existence of Weyl quasiparticles in a generic 3D system of dipolar particles in magnetic field, below we

focus on the experimentally important case of particles pinned in a deep unit-filled cubic lattice (Fig. 1a) with small lattice spacing a ; $ak_0 \ll 1$.

We assume that all particles are initially prepared in the $J_i = 0$ state and that the energy B_j of internal levels significantly exceeds the interaction strength (usually in dipolar gases^{30,35} $|\hat{H}_{\text{dip}}|/B_j \lesssim 10^{-6}$), leading to the conservation of the number of sites excited to the $J = 1$ state to a good accuracy (cf. ‘Methods’ section).

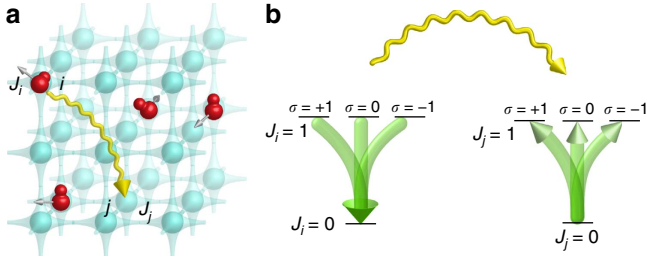


Figure 1 | Weyl quasiparticles in 3D dipolar arrays. (a) Schematics of the 3D lattice potential that traps an array of dipolar particles. The lattice is deep enough to pin the particles, most of which are prepared in the $J = 0$ ground state (blue spheres). Only a few particles are excited to the $J = 1$ states. Dipolar interactions between the $J = 0$ and $J = 1$ states give rise to Weyl excitations. (b) Schematics of dipole mediated interactions: an excited $J = 1$ state of one particle can be transferred to another particle in the $J = 0$ state by dipole-dipole interactions (virtual photon exchange is shown with a yellow wiggly line). Three types of allowed processes include $|00\rangle_i |1\sigma\rangle_j \leftrightarrow |1\sigma\rangle_i |00\rangle_j$, $|00\rangle_i |10\rangle_j \leftrightarrow |1, \pm 1\rangle_i |00\rangle_j$ and $|00\rangle_i |1, \pm 1\rangle_j \leftrightarrow |1, \mp 1\rangle_i |00\rangle_j$.

If an excitation with the angular momentum $J = 1$ is created on site i , the dipole-dipole interaction can transfer it to another site j , possibly changing the projection of the angular momentum on the direction of the magnetic field; $|1\sigma\rangle_i \rightarrow |1\sigma'\rangle_j$. The quasiparticles in the system are thus hard-core bosons corresponding to the angular-momentum degrees of freedom that hop from site to site as described by the effective Hamiltonian (see ‘Methods’ section for a detailed derivation)

$$\hat{H}_{\text{lat}} = \sum_{i,j,\sigma,\sigma'} M_{ij}^{\sigma\sigma'} \hat{b}_{i\sigma}^\dagger \hat{b}_{j\sigma'} = \sum_{\sigma\sigma'\mathbf{k}} M_{\mathbf{k}}^{\sigma\sigma'} \hat{b}_{\sigma,\mathbf{k}}^\dagger \hat{b}_{\sigma',\mathbf{k}}, \quad (6)$$

$$M_{ij}^{\sigma\sigma'} = \langle 1\sigma |_i \langle 00 |_j | \hat{H}_{\text{dip}} (\hat{\mathbf{d}}_i, \hat{\mathbf{d}}_j, \mathbf{r}_i - \mathbf{r}_j) | 00 \rangle_i | 1\sigma' \rangle_j - \sigma \delta_{\sigma\sigma'} \delta_{ij} B. \quad (7)$$

Due to the translational invariance, the single-excitation Hamiltonian can be diagonalised in the basis of momentum states \mathbf{k} , with the results shown in Fig. 2a,c. In accordance with the above general phenomenological argument, for $B \neq 0$ the dispersion has Weyl nodes (six in the first Brillouin zone, Fig. 2a,c).

To demonstrate the chiral nature of Weyl quasiparticles we show in Fig. 2d–f the pseudospins $\langle \hat{\sigma} \rangle$ (with the Pauli matrices $\hat{\sigma}_i$ acting in the space of the $J_z = -1$ and $J_z = 0$ angular-momentum projections) for the eigenstates with momenta \mathbf{k} in the horizontal ($p_z = 0$), tilted ($p_z = p_x$) and vertical ($p_x = 0$) planes (Fig. 2a) that contain a Weyl node. Excitations in these planes are equivalent to quasiparticles in graphene, the 2D counterpart of a Weyl semimetal, and are characterized by the non-trivial Berry phase π . Figure 2d–f demonstrates that the pseudospins $\hat{\sigma}$ of these states are linked to their momenta \mathbf{p} , measured from the Weyl node, in agreement with the effective Hamiltonian (2).

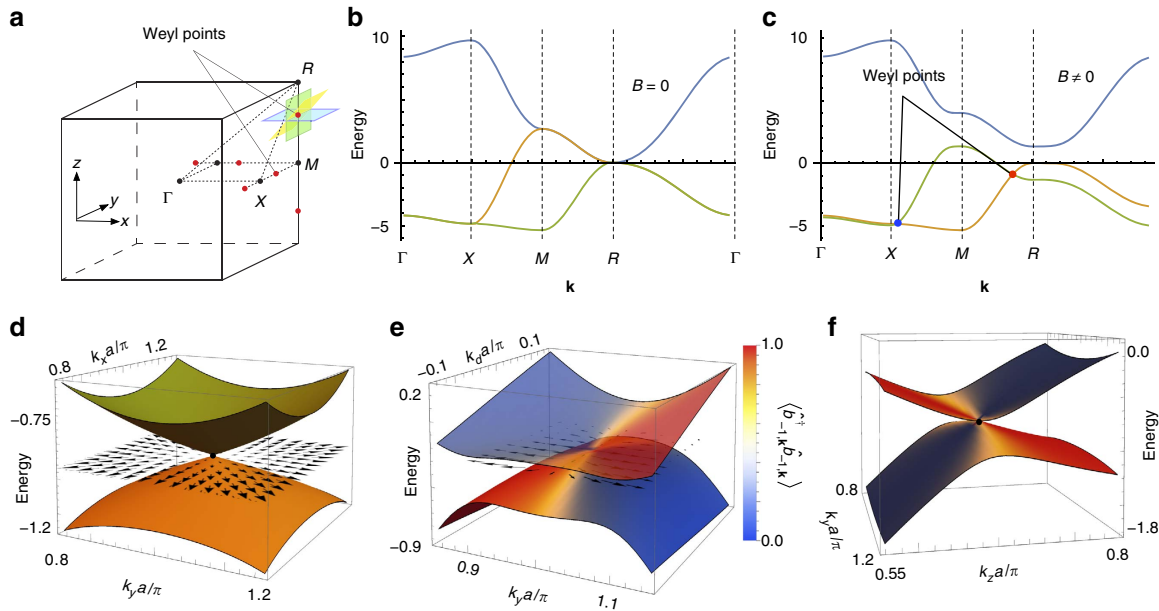


Figure 2 | Weyl quasi-particle dispersion and eigenstates. (a) Brillouin zone for the simple cubic lattice. (b) Dispersion along high-symmetry lines in the absence of magnetic field (all energies are measured in units of $(3/4)\gamma_0/(k_0 a)^3$). (c) Dispersion in the presence of magnetic field $B = \gamma_0/(k_0 a)^3$ demonstrating the existence of Weyl nodes (red points) with linear quasiparticle dispersion near them. Each node is characterized by the monopole charge ± 1 . In agreement with the fermion doubling theorem⁴⁴ (the Nielsen–Ninomiya no-go theorem), there is an even number (six) of Weyl points in the first Brillouin zone. (d) Dispersion in the horizontal ($k_x - k_y$) plane (shown by blue colour in panel (a)) containing the Weyl node near the R point. Quasiparticles in this plane are similar to quasiparticles in graphene and are characterized by a non-trivial Berry phase of π . The arrows show the pseudospin $\langle \hat{\sigma} \rangle$ (the Pauli matrices $\hat{\sigma}_i$ act in the space of the angular-momentum projections $J_z = 0$ and $J_z = -1$). (e) Dispersion along the (yellow in panel (a)) plane consisting of vectors $\mathbf{k} = (\pi + k_d/\sqrt{2}, \pi + k_y, 0.71\pi + k_d/\sqrt{2})$ containing the Weyl point. Colour shows the weight of the $|1 - 1\rangle$ state in the quasiparticle eigenstate, and arrows represent the pseudospin $\langle \hat{\sigma} \rangle$. (f) Dispersion along the (green in panel (a)) vertical plane ($k_y - k_z$) containing the Weyl point near the R point. For each momentum \mathbf{k} the colour represents the weight of the $|1 - 1\rangle$ state.

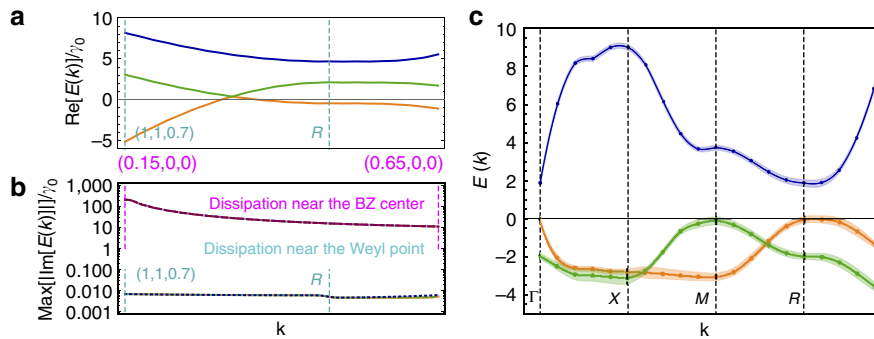


Figure 3 | Effects of disorder and dissipation on Weyl quasiparticles. (a) Real part of the quasiparticle dispersion in the presence of dissipation (including spontaneous emission and collective radiative decay). The parameters of the $J=1 \leftrightarrow J=0$ transition correspond to those of the electronic ${}^3P_0 - {}^3D_1$ levels of bosonic ${}^{88,84}\text{Sr}$ atoms, trapped in a magic optical lattice potential with $a = 206.4$ nm (ref. 35) at unit filling. Momentum \mathbf{k} is measured in units π/a . (b) The upper bound on the inelastic scattering rate estimated from simulating the full quasiparticle spectra including all allowed elastic and inelastic dipolar processes. The dissipation is significantly suppressed near the Weyl node (blue line). In striking contrast, the dissipation is enhanced close to the Γ point (red line) due to the enhanced collective emission (superradiance). (c) Disordered case: quasiparticle dispersion for a lattice with filling fraction $f = 0.93$ in the limit of small dissipation $k_0 a \ll 1$ (the energy is measured in units $\gamma_0/(k_0 a)^3$). The line thickness shows the inelastic scattering rate.

Effects of quenched disorder and dissipation. In general, quasiparticles in interacting systems have finite lifetimes due to elastic and inelastic scattering processes. Indeed, deep optical lattices under consideration are usually not completely filled by particles and thus inherently disordered due to the randomness of the particle distribution. Also, spontaneous and dipolar collective emission from the internal $J=1$ levels to the ground state can lead to the decay of the excitations.

To analyse the effects of dissipation in a unit-filled lattice we compute numerically the quasiparticle dispersion for retarded dipolar interactions, equation (5), with parameters of the $J=1$ to $J=0$ transition of the electronic ${}^3P_0 - {}^3D_1$ levels of bosonic ${}^{88,84}\text{Sr}$ atoms trapped in a magic optical lattice with $a = 206.4$ nm considered in ref. 35. The wavelength and the dipole moment for this transition are $2.6 \mu\text{m}$ and $d = 4.03D$, leading to the linewidth $\gamma_0 = 290 \times 10^3 \text{ s}^{-1}$ and the dissipation parameter $ak_0 \sim 0.5$. Albeit quasiparticle damping in this regime is rather strong, it is significantly suppressed (by more than three orders of magnitude) near the Weyl nodes, as our simulations show, Fig. 3a,b. Our results indicate that the quasiparticle scattering in such a system would be dominated by quenched disorder rather than by collective radiative decay or spontaneous emission.

To account for the effects of disorder we evaluate numerically the quasiparticle dispersion for a lattice filling of 93%. This filling fraction could be achieved by preparing a cold bosonic Mott insulator using moderate atom numbers that allow one to suppress doubly occupied states at the trap centre. Mott insulators have already been realised with bosonic AEA in the ground 1S_0 state^{36,37}. These atoms can be excited to the desired 3P_0 state by laser pulses³⁸.

As our simulations demonstrate, the characteristic energy scales of Weyl excitations significantly exceed the elastic scattering rate, demonstrating that the excitations could be conveniently observed in current experiments.

Experimental observation. For probing the Weyl character of the excitations we propose a Ramsey protocol illustrated in Fig. 4a. After preparing a Mott insulator of particles in the $J=0$ state, a pulse of interfering Raman beams is used to create excitations in the $|1, -1\rangle$ angular-momentum state with translational momentum \mathbf{k} . Here we consider the case when \mathbf{k} is set to be close to the Weyl point with intersecting $J_z = 0$ and $J_z = -1$ branches. For the proposed ${}^3P_0 - {}^3D_1$ electronic levels in Sr, two intermediate states $|e\rangle$, $|e'\rangle$ could be used to create the Raman pulses,

imparting a net momentum to the atoms proportional to $\mathbf{k} = \mathbf{k}_1 + \mathbf{k}_2 + \mathbf{k}_3$ (Fig. 4a). A possible excitation level scheme consists on using $5s6s {}^3S_1$ and $5s6p {}^3P_1$ as the intermediate $|e\rangle$ and $|e'\rangle$ levels respectively. After a waiting time t , another pulse is applied to measure the fraction of particles in the $J_z = 0$ angular-momentum state. Because of the interference of the two branches, this fraction oscillates with the frequency $(E_{\mathbf{k}}^1 - E_{\mathbf{k}}^2)/(2\pi)$, where the energy splitting $E_{\mathbf{k}}^1 - E_{\mathbf{k}}^2$ between the two branches is linear in \mathbf{k} and vanishes near the Weyl node.

Another signature of the Weyl node is the strong dependency of the amplitude of such oscillations on momentum \mathbf{k} near the node, as the amplitude is determined by the projection of the Bloch vector on \hat{k}_z (the magnetic field direction).

In Fig. 4c–f we show the fraction of particles in the $J_z = 0$ state as a function of time at the end of the above described Ramsey protocol, for the six different quasi-momenta in the $k_x - k_y$ plane near the Weyl point indicated in Fig. 4b. Figure 4c shows the dynamics for an ideal unit filled lattice in the dissipationless limit $k_0 a \ll 1$. Figure 4d shows the dynamics in the presence of dissipation for the experimentally relevant scenario discussed above. The population dynamics in disordered systems is shown in Figs 4e and 4f for 99% and 93% filled lattices respectively. Quasiparticles scattering on empty sites in a disordered system leads to the decay of the oscillations.

Discussion

We demonstrated that Weyl quasiparticles generically emerge in 3D systems of polar particles in magnetic field. This opens intriguing prospects of observing chiral anomaly, non-local electrodynamics, non-Anderson disorder-driven transitions, and other fascinating phenomena in the realm of fully controllable atomic systems. We showed that observing Weyl excitations is currently possible in arrays of AEA in 3D lattices, in particular, using the ${}^3P_0 - {}^3D_1$ levels of bosonic Sr atoms. Other experimentally convenient schemes, that deserve further exploration, include using metastable levels of Sr or Yb atoms that can be trapped in magic lattices with spacings smaller than the wavelength³⁹ or arrays of polar molecules with the rotational levels dressed to avoid the splitting of $J=1$ levels in the presence of hyperfine interactions³⁰. The long lifetimes and the topological character of Weyl excitations in interacting dipolar systems also open new possibilities for implementing optical-lattice clocks with sensing capabilities beyond those of non-interacting systems.

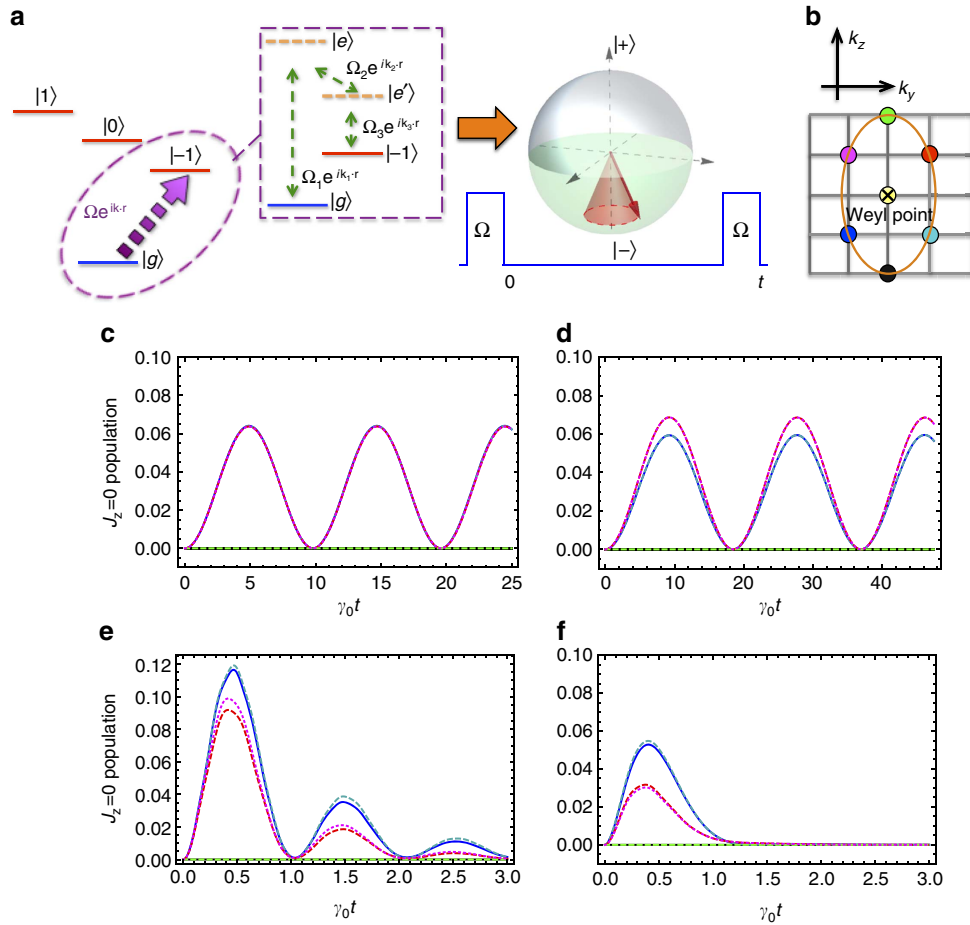


Figure 4 | Observation of Weyl quasiparticles. (a) Momentum-selective Ramsey spectroscopy: interfering Raman beams create an excitation with the angular-momentum projection $J_z = -1$ and with translational momentum \mathbf{k} near the Weyl node (see text). After a waiting time t the second pulse is applied to measure the fraction of particles in the $J_z = 0$ angular-momentum state. (b) Six quasimomenta near the Weyl node. (c) The fraction of particles in the $J_z = 0$ state oscillates as a function of time t with the frequency $(E_{\mathbf{k}}^1 - E_{\mathbf{k}}^2)/(2\pi)$, where $E_{\mathbf{k}}^1 - E_{\mathbf{k}}^2$ is the energy splitting between the two branches of the quasiparticle dispersion. (d) The oscillations in the presence of dissipation for $k_0 a \sim 0.5$. (e) The oscillations in a 99% randomly filled lattice. (f) The oscillations in a 93% filled lattice. For (c,d) a 3D cubic lattice of $100 \times 100 \times 100$ sites was used and we took advantage of the translational symmetry. For (e,f) a 3D cubic lattice of $10 \times 10 \times 10$ was used.

Methods

Dispersion near Weyl nodes. In this work, we define the quasiparticle dispersion as the poles of the retarded Green’s function averaged with respect to quenched disorder.

While long-wave quasiparticles ($\mathbf{k} \rightarrow 0$) are insensitive to the details of the lattice potential, their effective Hamiltonian preserves rotation and inversion symmetries, and in the absence of magnetic field– time-reversal symmetry, with the generic form of the Hamiltonian given by equation (1) and with the vector ω parallel to the magnetic field.

We assume the existence of excitations with momentum $J=1$ and focus on the respective manifold of states in what follows. The dispersion of such excitations has three branches for each momentum \mathbf{k} .

For momenta \mathbf{k} parallel to ω the respective excitations have momentum projections $J_z = 0$ and $J_z = \pm 1$ on the direction ω . The branch with $J_z = 0$ intersects the branch with $J_z = \pm 1$ at momenta $\mathbf{K} \parallel \omega$ such that

$$F(|\mathbf{K}|, K^2, 2) \pm \omega = F(|\mathbf{K}|, 0, 2), \tag{8}$$

where we used that $\hat{J}^2 = J(J+1) = 2$ for the states under consideration.

The quasiparticle dispersion near the nodes can be found by expanding the Hamiltonian in small momenta $\mathbf{p} = \mathbf{k} - \mathbf{K}$. Momentum deviation from a node along the z axis leads to the splitting $F[K+p_z, (K+p_z)^2, 2] \pm \omega - F[K+p_z, 0, 2]$ between the intersecting branches. Using that $[(\mathbf{K} + \mathbf{p}) \cdot \hat{\mathbf{J}}]^2 \approx \frac{K_x^2}{2} + \frac{K_y^2}{2} \hat{\sigma}_z + Kp_z + Kp_z \hat{\sigma}_z \pm \frac{K}{\sqrt{2}} (p_x \hat{\sigma}_x + p_y \hat{\sigma}_y)$, with $\hat{\sigma}_i$ being the Pauli matrices in the space of momentum projections $J_z = +1$ ($J_z = -1$) and

$J_z = 0$, we obtain the quasiparticle Hamiltonian (2) with

$$\zeta(\mathbf{p}) = \frac{1}{2} F[K+p_z, (K+p_z)^2, 2] - \frac{1}{2} F[K, K^2, 2] + \frac{1}{2} F[K+p_z, 0, 2] - \frac{1}{2} F(K, 0, 2), \tag{9}$$

$$v_{\perp} = \pm \frac{1}{\sqrt{2}} KF^{(2)}(K, K^2, 2) \tag{10}$$

$$v_{\parallel} = KF^{(2)}(K, K^2, 2) + \frac{1}{2} [F^{(1)}(K, K^2, 2) - F^{(1)}(K, 0, 2)] \tag{11}$$

where the upper (lower) sign in equation (10) applies to the intersection of the $J_z = 0$ branch with $J_z = +1$ ($J_z = -1$), and $F^{(1)}$ and $F^{(2)}$ are the derivatives of the function F with respect to the first and the second argument.

Generic Hamiltonian of retarded dipole-dipole interactions. The dynamics of internal transitions $J=0 \leftrightarrow J=1$ in a system of N particles is described by the Hamiltonian

$$\hat{H} = \sum_{j=1}^N \Delta \hat{c}_j^\dagger \cdot \hat{c}_j + \sum_{\mathbf{q}^\lambda} \omega_{\mathbf{q}} \hat{a}_{\mathbf{q},\lambda}^\dagger \hat{a}_{\mathbf{q},\lambda} + d \sum_{j=1}^N \mathbf{E}(\mathbf{r}_j) \cdot (\hat{c}_j^\dagger + \hat{c}_j), \tag{12}$$

where the operator $\hat{c}_j^{\alpha\dagger} = |\alpha\rangle \langle 0|$ excites the j -th atom from the ground state $|0\rangle$ to one of the Cartesian states $\alpha = x, y, z$ of the $J=1$ manifold with energy Δ ; d is the dipole moment of such a transition; $\hat{a}_{\mathbf{q},\lambda}^\dagger$ and $\hat{a}_{\mathbf{q},\lambda}$ are the creation and annihilation

operators of a photon with momentum \mathbf{q} , frequency ω , and polarization λ ; $\mathbf{E}(\mathbf{r}) = i \sum_{\mathbf{q}, \lambda} \sqrt{\frac{\omega_{\mathbf{q}}}{2\epsilon_0 V}} \hat{\mathbf{e}}_{\mathbf{q}, \lambda} (\hat{a}_{\mathbf{q}, \lambda} e^{-i\mathbf{q} \cdot \mathbf{r}} - \hat{a}_{\mathbf{q}, \lambda}^\dagger e^{i\mathbf{q} \cdot \mathbf{r}})$ is the operator of electric field and V is the volume of the system.

Eliminating the electromagnetic-field modes gives in the Born–Markov approximation the master equation for the density matrix of the particles^{28,40}

$$\dot{\hat{\rho}} = -i[\hat{H}_0 + \hat{H}^{\text{el}}, \hat{\rho}] + \mathcal{D}(\hat{\rho}), \quad (13)$$

where $\hat{H}_0 = \sum_{j=1}^N \Delta \hat{c}_j^\dagger \cdot \hat{\mathbf{c}}_j$ is the Hamiltonian of the internal states of the particles, and the effective interaction Hamiltonian is given by

$$\hat{H}_{j,k}^{\text{el}} = \sum_{j \neq k} \left(A(r_{jk}) (\hat{\mathbf{r}}_{jk} \cdot \hat{\mathbf{d}}_j) (\hat{\mathbf{r}}_{jk} \cdot \hat{\mathbf{d}}_k) + B(r_{jk}) \hat{\mathbf{d}}_j \cdot \hat{\mathbf{d}}_k \right) \quad (14)$$

with $A(r) = \frac{3j_0}{4\pi\epsilon_0} y_2(k_0 r)$, $B(r) = \frac{3j_0}{4\pi\epsilon_0} \sum_{n=0}^1 (-1)^n y_n(k_0 r)/(k_0 r)$ and y_n being the n -th-order spherical Bessel function of the second kind, k_0 is the wavevector of the $J=0$ to $J=1$ transition, $\hat{\mathbf{d}}_j \equiv \hat{a}_{j,1}^\dagger \hat{a}_{j,0}$, $\mathbf{r}_{jk} = \mathbf{r}_j - \mathbf{r}_k$, $r_{jk} = |\mathbf{r}_{jk}|$, and $\hat{\mathbf{r}}_{jk} = \mathbf{r}_{jk}/r_{jk}$.

The operator $\mathcal{D}(\hat{\rho})$ in equation (13) accounts for dissipation and is given by

$$\mathcal{D}(\hat{\rho}) = -i \sum_{j,k} \left[(\hat{H}_{j,k}^{\text{di}} \hat{\rho} - \hat{\rho} \hat{H}_{j,k}^{\text{di}*}) + \Upsilon_{j,k} \right] \quad (15)$$

where $\hat{H}_{j,k}^{\text{di}} = \mathcal{A}(r_{jk}) (\hat{\mathbf{r}}_{jk} \cdot \hat{\mathbf{d}}_j) (\hat{\mathbf{r}}_{jk} \cdot \hat{\mathbf{d}}_k) + \mathcal{B}(r_{jk}) \hat{\mathbf{d}}_j \cdot \hat{\mathbf{d}}_k$, $\mathcal{A}(r) = -i \frac{3j_0}{4\pi\epsilon_0} y_2(k_0 r)$, $\mathcal{B}(r) = -i \frac{3j_0}{4\pi\epsilon_0} \sum_{n=0}^1 (-1)^n J_n(k_0 r)/(k_0 r)$, with J_n being the n -th-order spherical Bessel function of the first kind, and $\Upsilon_{j,k} \propto \hat{\mathbf{c}}_j \cdot \mathcal{T}_{j,k} \cdot \hat{\mathbf{c}}_k^\dagger$ is the so-called recycling operator²⁸ that does not affect the dynamics of a single excitation and is thus omitted in the present paper. Combining the interaction $\hat{H}_{j,k}^{\text{el}}$ and dissipation $\hat{H}_{j,k}^{\text{di}}$ terms we obtain the effective (non-Hermitian) Hamiltonian (5) of the dipole–dipole interactions.

Excitation dispersion in a deep lattice. As particles cannot move from site to site in a deep optical lattice, the quasiparticles are represented by the angular-momentum degrees of freedom that propagate through the system. Assuming there is one particle per site and introducing bosonic operators $\hat{d}_{i\sigma}^\dagger$ and $\hat{d}_{i\sigma}$ for creating and annihilating the particle state $|1\sigma\rangle_i$ on site i with angular momentum $J=1$ and projection σ and the operators \hat{a}_i^\dagger and \hat{a}_i for creating and annihilating the momentum state $J=0$ on site i , the system Hamiltonian can be rewritten as

$$\begin{aligned} \hat{H} = & \sum_{i,j,\sigma,\sigma'} \langle 1\sigma|_i \langle 00|_j \hat{H}_{\text{dip}}(\hat{\mathbf{d}}_i, \hat{\mathbf{d}}_j; \mathbf{r}_{ij}) |00\rangle_i |1\sigma'\rangle_j \hat{d}_{i\sigma}^\dagger \hat{d}_{j\sigma'} \hat{a}_i^\dagger \hat{a}_j \\ & + \sum_{i,j,\sigma,\sigma'} \left[\langle 1\sigma|_i \langle 1\sigma'|_j \hat{H}_{\text{dip}}(\hat{\mathbf{d}}_i, \hat{\mathbf{d}}_j; \mathbf{r}_{ij}) |00\rangle_i |00\rangle_j \hat{d}_{i\sigma}^\dagger \hat{d}_{j\sigma'} \hat{a}_i^\dagger \hat{a}_j \hat{a}_i^\dagger \right. \\ & + \langle 00|_i |00\rangle_j \hat{H}_{\text{dip}}(\hat{\mathbf{d}}_i, \hat{\mathbf{d}}_j; \mathbf{r}_{ij}) |1\sigma\rangle_i |1\sigma'\rangle_j \hat{d}_{i\sigma}^\dagger \hat{d}_{j\sigma'} \hat{a}_i^\dagger \hat{a}_j \left. \right] \\ & - B \sum_{i\sigma} \sigma \hat{a}_{i\sigma}^\dagger \hat{d}_{i\sigma} \hat{a}_i \hat{a}_i^\dagger + B_j \sum_{i\sigma} \hat{a}_{i\sigma}^\dagger \hat{d}_{i\sigma} \\ & + U \sum_{i\sigma} \left[\hat{a}_{i\sigma}^\dagger \hat{d}_{i\sigma} (\hat{d}_{i\sigma}^\dagger \hat{d}_{i\sigma} - 1) + \hat{a}_i^\dagger \hat{a}_i (\hat{a}_i^\dagger \hat{a}_i - 1) \right. \\ & \left. + \hat{d}_{i\sigma}^\dagger \hat{d}_{i\sigma} \hat{a}_i^\dagger \hat{a}_i \right]. \end{aligned} \quad (16)$$

The first term in the Hamiltonian (16) is responsible for moving angular-momentum excitations from site to site; the angular-momentum state $|1\sigma\rangle_i$ can be transferred by the dipole–dipole interactions from site i to another state $|1\sigma'\rangle_j$ on site j that initially was in the $J=0$ state. The terms in the second sum in equation (16) change pairs of sites i and j from the $J=0$ to $J=1$ angular-momentum states or vice versa. The term $\propto B$ is the Zeeman energy. The term $\propto B_j$ accounts for the internal rotation (internal levels) of the particles. The terms $\propto U = \infty$ in equation (16) enforce the hard-core constraints for the bosons created by the operators $\hat{d}_{i\sigma}^\dagger$ and \hat{a}_i^\dagger , taking into account that there is one particle on each site.

In this paper we consider excitations on top of the ground state with all sites (particles) in the $J=0$ state. Exciting the internal degree of freedom of a particle on a site costs the rotation energy B_j that significantly exceeds all the other energy scales, except $U = \infty$, including the matrix elements $\sim |\hat{H}_{\text{dip}}|$ of hopping of such angular-momentum degrees of freedom between sites (for instance, for dipolar molecules and AEs $|\hat{H}_{\text{dip}}|/B_j \lesssim 10^{-6}$). As a result, the number of sites excited to the $J=1$ states is conserved to a good approximation, and the second sum in equation (16), that creates or annihilates pairs of $J=1$ excitations, can be neglected when considering the angular-momentum dynamics.

Therefore, the quasiparticles in the system are hard-core bosons that carry angular-momentum ($J=1$) degrees of freedom and hop from site to site as described by the effective Hamiltonian (6) and (7) with $\hat{b}_{i\sigma} = \hat{d}_{i\sigma} \hat{a}_i^\dagger$.

Details of disorder averaging. Realistic systems of particles pinned in deep optical lattices are inherently disordered due to the randomness of the spatial distribution of the particles. Each lattice site hosts either a particle with probability f or a vacancy with probability $1-f$.

For a small concentration of vacancies, excitations in the system are delocalized and their dispersion is close to that in the disorder-free system but acquires a small finite imaginary part $\text{Im}E_{\mathbf{k}}$ due to the scattering on the vacancies.

To numerically obtain the quasiparticle spectra in such a disordered system we diagonalize the Hamiltonian $\hat{\mathcal{H}} = \hat{\mathcal{H}}_0 + \hat{V}$, where $\hat{\mathcal{H}}_0$ is the excitation Hamiltonian in the clean case and the operator \hat{V} models vacancies as sites with infinite potential $V(\mathbf{r}_i) = \infty$. We compute the retarded Green’s function

$$G(\mathbf{r}_1\sigma_1, \mathbf{r}_2\sigma_2, E) = \sum_{\alpha} \frac{\psi_{2\sigma_2}^*(\mathbf{r}_1) \psi_{2\sigma_1}(\mathbf{r}_2)}{E - E_{\alpha} + i\eta} \quad (17)$$

for multiple disorder realizations, where ψ_{α} and E_{α} are the eigenfunctions and eigenenergies for a particular disorder realization, σ_1 and σ_2 label projections of the angular momentum $J=1$, and η is a small positive number introduced to ensure that the disorder-averaged Green’s function $\langle G(\mathbf{r}_1\sigma_1, \mathbf{r}_2\sigma_2, E) \rangle_{\text{dis}}$ is a smooth function of its arguments for a given number of disorder realizations. At the same time, η has to be chosen sufficiently small to not affect the results for the quasiparticle dispersion. The energy E has to be chosen close to the energies of the quasiparticles of interest.

Disorder averaging restores translational invariance, yielding an averaged Green’s function that depends only on the coordinate difference $\mathbf{r}_2 - \mathbf{r}_1$. Computing the Fourier transform of the function $\langle G(\mathbf{r}_1\sigma_1, \mathbf{r}_2\sigma_2, E) \rangle_{\text{dis}}$ with respect to $\mathbf{r}_2 - \mathbf{r}_1$ and diagonalising it in the angular-momentum space gives $1/(E - E_{k\eta})$, where $n=1, 2, 3$ labels the dispersion branch for a given \mathbf{k} , $\text{Re}E_{k\eta}$ is the quasiparticle dispersion and $-2\text{Im}E_{k\eta}$ is the scattering rate.

In this paper we perform averaging over 100 disorder realizations on a $10 \times 10 \times 10$ cubic lattice with periodic boundary conditions for the filling fraction $f=0.93$, close to that in the recent experiments^{41–43}. The results for the quasiparticle dispersion and scattering rates are shown in Fig. 3c.

Data availability. The datasets generated in the current study are available from the corresponding author on reasonable request.

References

- Burkov, A. A. & Balents, L. Weyl semimetal in a topological insulator multilayer. *Phys. Rev. Lett.* **107**, 127205 (2011).
- Wan, X., Turner, A. M., Vishwanath, A. & Savrasov, S. Y. Topological semimetal and Fermi-arc surface states in the electronic structure of pyrochlore iridates. *Phys. Rev. B* **83**, 205101 (2011).
- Lu, L. *et al.* Experimental observation of Weyl points. *Science* **349**, 622 (2015).
- Ly, B. Q. *et al.* Experimental discovery of Weyl semimetal TaAs. *Phys. Rev. X* **5**, 031013 (2015).
- Xu, S.-Y. *et al.* Discovery of a Weyl fermion semimetal and topological Fermi arcs. *Science* **349**, 613 (2015).
- Parameswaran, S. A., Grover, T., Abanin, D. A., Pesin, D. A. & Vishwanath, A. Probing the chiral anomaly with nonlocal transport in three-dimensional topological semimetals. *Phys. Rev. X* **4**, 031035 (2014).
- Fradkin, E. Critical behavior of disordered degenerate semiconductors. I. models, symmetries, and formalism. *Phys. Rev. B* **33**, 3257 (1986).
- Goswami, P. & Chakravarty, S. Quantum criticality between topological and band insulators in 3+1 dimensions. *Phys. Rev. Lett.* **107**, 196803 (2011).
- Kobayashi, K., Ohtsuki, T., Imura, K.-I. & Herbut, I. F. Density of states scaling at the semimetal to metal transition in three dimensional topological insulators. *Phys. Rev. Lett.* **112**, 016402 (2014).
- Moon, E.-G. & Kim, Y. B. Non-Fermi liquid in Dirac semi-metals. arXiv:1409.0573 (2014).
- Sbierski, B., Pohl, G., Bergholtz, E. J. & Brouwer, P. W. Quantum transport of disordered Weyl semimetals at the nodal point. *Phys. Rev. Lett.* **113**, 026602 (2014).
- Syzranov, S. V., Gurarie, V. & Radzihovsky, L. Unconventional localisation transition in high dimensions. *Phys. Rev. B* **91**, 035133 (2015).
- Syzranov, S. V., Radzihovsky, L. & Gurarie, V. Critical transport in weakly disordered semiconductors and semimetals. *Phys. Rev. Lett.* **114**, 166601 (2015).
- Rodionov, Y. I. & Syzranov, S. V. Conductivity of a Weyl semimetal with donor and acceptor impurities. *Phys. Rev. B* **91**, 195107 (2015).
- Sarma, S. D., Hwang, E. H. & Min, H. Carrier screening, transport, and relaxation in 3D Dirac semimetals. *Phys. Rev. B* **91**, 035201 (2015).
- Skinner, B. Coulomb disorder in three-dimensional Dirac systems. *Phys. Rev. B* **90**, 062022 (2014).
- Anderson, B. M., Juzeliūnas, G., Galitski, V. M. & Spielman, I. B. Synthetic 3D spin-orbit coupling. *Phys. Rev. Lett.* **108**, 235301 (2012).
- Dubček, T. *et al.* Weyl points in three-dimensional optical lattices: synthetic magnetic monopoles in momentum space. *Phys. Rev. Lett.* **114**, 225301 (2015).
- Ganeshan, S. & Sarma, S. D. Constructing a Weyl semimetal by stacking one-dimensional topological phases. *Phys. Rev. B* **91**, 125438 (2015).
- Jiang, J.-H. Tunable topological Weyl semimetal from simple-cubic lattices with staggered fluxes. *Phys. Rev. A* **85**, 033640 (2012).

21. Lan, Z., Goldman, N., Bermudez, A., Lu, W. & Öhberg, P. Dirac-Weyl fermions with arbitrary spin in two-dimensional optical superlattices. *Phys. Rev. B* **84**, 165115 (2011).
22. Liu, B., Li, X., Yin, L. & Liu, W. V. Weyl superfluidity in a three-dimensional dipolar Fermi gas. *Phys. Rev. Lett.* **114**, 045302 (2015).
23. Gong, M., Tewari, S. & Zhang, C. BCS-BEC crossover and topological phase transition in 3d spin-orbit coupled degenerate fermi gases. *Phys. Rev. Lett.* **107**, 195303 (2011).
24. Seo, K., Han, L. & Sá de Melo, C. A. Emergence of majorana and dirac particles in ultracold fermions via tunable interactions, spin-orbit effects, and zeeman fields. *Phys. Rev. Lett.* **109**, 105303 (2012).
25. Xia-Ji, L., Hui, H. & Han., P. Three-dimensional spinorbit coupled fermi gases: fuldeferrell pairing, majorana fermions, weyl fermions, and gapless topological superfluidity. *Chin. Phys. B* **24**, 050502 (2015).
26. Weyl, H. Elektron und gravitation. I. *Z. Phys.* **56**, 330 (1929).
27. Bloom, B. J. *et al.* An optical lattice clock with accuracy and stability at the 10^{-18} level. *Nature* **506**, 71–74 (2014).
28. Gross, M. & Haroche, S. Superradiance: an essay on the theory of collective spontaneous emission. *Phys. Rep.* **93**, 301 (1982).
29. Childress, L. Diamond dynamics under control. *Science* **345**, 1247 (2015).
30. Yan, B. *et al.* Observation of dipolar spin-exchange interactions with lattice-confined polar molecules. *Nature* **501**, 521–525 (2013).
31. Robicheaux, F., Hernandez, J. V., Topcu, T. & Noordam, L. D. Simulation of coherent interactions between Rydberg atoms. *Phys. Rev. A* **70**, 042703 (2004).
32. Weber, T. M. *et al.* Mesoscopic Rydberg-blockaded ensembles in the superatom regime and beyond. *Nat. Phys.* **11**, 157 (2015).
33. Novoselov, K. S. *et al.* Electric field effect in atomically thin carbon films. *Science* **306**, 666–669 (2004).
34. Syzranov, S. V., Wall, M. L., Gurarie, V. & Rey, A. M. Spin-orbital dynamics in a system of polar molecules. *Nat. Commun.* **5**, 5391 (2014).
35. Olmos, B. *et al.* Long-range interacting many-body systems with alkaline-earth-metal atoms. *Phys. Rev. Lett.* **110**, 143602 (2013).
36. Stellmer, S., Schreck, F. & Killian, T. C. *Degenerate Quantum Gases of Strontium* Vol. 2, 1–80 (World Scientific Publishing Co., 2014).
37. Sugawa, S., Takasu, Y., Enomoto, K. & Takahashi, Y. *Ultracold Ytterbium: Generation, Many-Body Physics, and Molecules*. Vol. 1 3–51 (World Scientific Publishing Co., 2013).
38. Akatsuka, T., Takamoto, M. & Katori, H. Optical lattice clocks with non-interacting bosons and fermions. *Nature* **4**, 954–959 (2008).
39. Safronova, M. S., Zuhrianda, Z., Safronova, U. I. & Clark, C. W. The magic road to precision. arXiv:1507.06570 (2015).
40. James, D. F. V. Frequency shifts in spontaneous emission from two interacting atoms. *Phys. Rev. A* **47**, 1336 (1993).
41. Greif, D., Uehlinger, T., Jotzu, G., Tarruell, L. & Esslinger, T. Short-range quantum magnetism of ultracold fermions in an optical lattice. *Science* **340**, 1307–1310 (2013).
42. Köhl, M., Moritz, H., Stöferle, T., Günter, K. & Esslinger, T. Fermionic atoms in a three dimensional optical lattice: observing Fermi surfaces, dynamics, and interactions. *Phys. Rev. Lett.* **94**, 080403 (2005).
43. Schneider, U. *et al.* Metallic and insulating phases of repulsively interacting fermions in a 3D optical lattice. *Science* **322**, 1520–1525 (2008).
44. Nielsen, H. B. & Ninomiya, M. Absence of neutrinos on a lattice (I). Proof by homotopy theory. *Nucl. Phys. B* **185**, 20 (1981).

Acknowledgements

We thank M. Hermele and J. Ye for useful discussions and R. Nandkishore for feedback on the manuscript. This work was supported by the NSF (PIF-1211914, PFC-1125844 and DMR-1205303), AFOSR, AFOSR-MURI, NIST and ARO. MLW thanks the NRC postdoctoral fellowship programme for support. SVS has been also partially supported by the Alexander von Humboldt Foundation through the Feodor Lynen Research Fellowship.

Author contributions

All authors contributed to all aspects of this work.

Additional information

Competing financial interests: The authors declare no competing financial interests.

Reprints and permission information is available online at <http://npg.nature.com/reprintsandpermissions/>

How to cite this article: Syzranov, S. V. *et al.* Emergent Weyl excitations in systems of polar particles. *Nat. Commun.* **7**, 13543 doi: 10.1038/ncomms13543 (2016).

Publisher's note: Springer Nature remains neutral with regard to jurisdictional claims in published maps and institutional affiliations.



This work is licensed under a Creative Commons Attribution 4.0 International License. The images or other third party material in this article are included in the article's Creative Commons license, unless indicated otherwise in the credit line; if the material is not included under the Creative Commons license, users will need to obtain permission from the license holder to reproduce the material. To view a copy of this license, visit <http://creativecommons.org/licenses/by/4.0/>

© The Author(s) 2016